# Fluctuations in populations of subsurface methane oxidizers in coordination with changes in electron acceptor availability

C. Magnabosco[1*], P.H.A. Timmers[2], M.C.Y. Lau[3], G. Borgonie[4], B. Linage-Alvarez[5], O. Kuloyo[5,6], R. Alleva[7], T.L. Kieft[8], G.F. Slater[9], E. van Heerden[5,10], B. Sherwood Lollar[11], T.C. Onstott[3]

[1]Flatiron Institute Center for Computational Biology, Simons Foundation, New York USA
[2]Department of Microbial Physiology, Laboratory of Microbiology, Wageningen University, Wageningen Netherlands
[3]Department of Geosciences, Princeton University, Princeton USA
[4]Extreme Life Isyensya, Gentbrugge Belgium
[5] Department of Microbial, Biochemical and Food Biotechnology, University of the Free State Bloemfontein, South Africa
[6]Department of Geoscience, University of Calgary, Calgary Canada
[7]Department of Ecology and Evolutionary Biology, Princeton University, Princeton USA
[8]Department of Biology, New Mexico Institute of Mining and Technology, Socorro USA
[9]School of Geography and Earth Sciences, McMaster University, Hamilton Canada
[10]Biosaense Solutions, Bloemfontein, South Africa
[11]Department of Earth Sciences, University of Toronto, Toronto Canada
*To whom correspondence should be addressed: Cara Magnabosco; 162 Fifth Ave, New York, NY 10012
cmagnabosco@flatironinstitute.org; +1 646-603-3683

**Running Title:** Subsurface ANME in South Africa

**Abstract:**

The concentrations of electron donors and acceptors in the terrestrial subsurface biosphere fluctuate due to migration and mixing of subsurface fluids, but the mechanisms and rates at which microbial communities respond to these changes are largely unknown. Subsurface microbial communities exhibit long cellular turnover times and are often considered relatively static—generating just enough ATP for cellular maintenance. Here, we investigated how subsurface populations of $CH_4$ oxidizers respond to changes in electron acceptor availability by monitoring the biological and geochemical composition in a 1,339 meters-below-land-surface (mbls) fluid-filled fracture over the course of both longer (2.5 year) and shorter (2-week) time scales. Using a combination of metagenomic, metatranscriptomic, and metaproteomic analyses, we observe that the $CH_4$ oxidizers within the subsurface microbial community change in coordination with electron acceptor availability over time. We then validate these findings through a series of $^{13}C$-$CH_4$ laboratory incubation experiments, highlighting a connection between composition of subsurface $CH_4$ oxidizing communities and electron acceptor availability.

**Introduction:**

The terrestrial subsurface is an energy-limited environment that is subject to changes in fluid chemistry over time (Onstott *et al.* 2006). Laboratory experiments have shown that when native fluids are supplemented with electron acceptors such as $SO_4^{2-}$, the activity of subsurface communities can be enhanced (Rajala *et al.* 2015). Large disturbances such as $CO_2$ (Morozova *et al.* 2010, 2011) and $H_2$ injection (Bagnoud *et al.* 2016), hydraulic fracking (Daly *et al.* 2016), and drilling (Purkamo *et al.* 2013) have also

been reported to alter natural subsurface communities. The response of microbial communities to natural fluctuations in their environment, however, is less understood.

In the South African subsurface, increases in the availability of electron acceptors such as $NO_3^-$ (>10-fold higher) and $SO_4^{2-}$ (>5-fold higher) over a 1.5 year period did not correspond to changes in the bacterial community (Magnabosco *et al.* 2014; Simkus *et al.* 2015). However, 16S SSU rRNA gene amplicon surveys of the archaeal communities from the same site and sampling points of the aforementioned studies showed a diverse collection of anaerobic methane oxidizing archaea (ANME) (Young *et al.* 2017) and methane oxidizing bacteria (Simkus *et al.* 2015).

ANME-1 and "*Candidatus* Methanoperedens nitroreducens", a member of ANME-2d, are among the best described ANME and couple the oxidation of $CH_4$ with $SO_4^{2-}$ and $NO_3^-$ reduction, respectively (Haroon *et al.* 2013; Wegener *et al.* 2015). Other ANME-2d have also been reported to couple $CH_4$ oxidation to the reduction of $Mn^{4+}$ and/or $Fe^{3+}$ (Ettwig *et al.* 2016). With the exception of "*Ca.* Methylomirabilis oxyfera" which has been suggested to generate intracellular $O_2$ for $CH_4$ oxidation from two molecules of NO (Ettwig *et al.* 2010), bacterial methanotrophs couple $CH_4$ oxidation with free $O_2$ in the environment. This potential relationship between $CH_4$ oxidizers (MOs) and electron acceptor availability provides a compelling avenue to explore the response of subsurface communities to natural changes in subsurface fluid chemistry.

Our study focuses on the subsurface microbial community of a 1,339 meters-below-land-surface (mbls) fluid-filled fracture (Be326 Bh2). Here, bulk bacterial phospholipid-derived fatty acid (PLFA) isotopic signatures have been shown to be consistent with the accumulation of $^{13}C$-dissolved inorganic carbon (DIC) impacted by the microbial oxidation of $CH_4$ (Simkus *et al.* 2015) but the organisms responsible for $CH_4$ oxidation have not been well characterized (Magnabosco *et al.* 2014; Simkus *et al.* 2015; Young *et al.* 2017). To better describe the membership of native MO communities, their methane oxidizing genes, and their response to changes in fluid chemistry over time, we combined metagenomics, metatranscriptomics, and metaproteomics analyses with geochemical monitoring of Be326 Bh2's *in situ* fracture fluids over both 2.5 year and 2 week timescales. We also performed activity assays on the fracture fluids using $^{13}C$-labeled $CH_4$ together with different electron acceptors to track anaerobic methane oxidizing activity in both short- and long-term incubations.

## Materials and Methods:

Be326 Bh2 was accessed through a 57-m, horizontally drilled borehole that was drilled in 2007 and sealed with a high-pressure steel valve. The borehole is located on the 26 level of shaft 3 in the Beatrix Gold Mine (28.232288 S, 26.794365 E; Welkom, South Africa). Annual samples were collected during field trips in 2011, 2012, and 2013 and weekly samples were collected during the 2013 field trip with three time points designated as $T_0$, $T_1$, and $T_2$ with $T_0$ corresponding to the first day of the 2013 study and $T_2$ corresponding to the last day of the 2013 study.

### *Sampling*

Sampling procedures have been outlined previously (Magnabosco *et al.* 2014). To sample, a sterile (combusted and autoclaved) stainless steel manifold with attached valves was attached to the Be326 borehole. A high-pressure steel valve was opened, allowing water to flow freely at ~4-6 L $min^{-1}$ for at least 10 minutes. This manifold allows for the

95 attachment of airtight Teflon tubing and filters for sampling and chemical analysis. For
96 the 2011, 2012, and 2013 samples, pre-autoclaved 0.1-µm Memtrex NY filters (MNY-91-
97 1-AAS; General Electric Co., Minnetonka, MN USA) were left on the borehole for 6, 15,
98 and 14 days, respectively. For the $T_0$, $T_1$, and $T_2$ samples, 0.2-µm Memtrex NY Capsule
99 (CMNY) filters (General Electric Co., Minnetonka, MN USA) were left on the borehole
100 for 2 hours with a flow rate of 500 mL per minute (equivalent to approximately 60 L
101 filtered per time point) in 2013. The total volumes of water filtered for each time point in
102 the 2.5-year study were 4,875 L, 12,604 L, and 6,635 L in 2011, 2012 and 2013,
103 respectively.
104 Unfiltered water samples for direct cell counts were collected on the first day of
105 the 2011, 2012, and 2013 studies and fixed with sterile formaldehyde (final concentration
106 4% v/v). Cell counts were obtained at the University of the Free State where samples
107 were filtered through a sterile 0.22µm Millipore GTTP-type membrane filter, stained
108 with DAPI, and visualized using fluorescence microscopy.
109 ***Geochemical Measurements***
110 Temperature, pH, and $E_h$ were measured at the borehole using handheld probes
111 (HANNA instruments, Woonsocket, RI). Gas samples ($H_2$, $O_2$, $CH_4$) were collected and
112 analyzed by gas chromatography (Peak Performer 1 series, Peak Laboratories, USA)
113 (Simkus *et al.* 2015). Oxygen was also measured at the borehole using a CHEMET kit
114 (Chemetrics Inc.; Calverton, VA). $NO_3^-$ and $SO_4^{2-}$ were measured using an ion
115 chromatograph coupled to an electrospray ionization-quadruple mass spectrometer (MS)
116 (Dionex IC25 and Thermo Scientific MSQ, USA). $\delta^{18}O$ and $\delta^2H$ were measured as
117 previously described (Simkus *et al.* 2015).
118 ***Preservation of Biomolecules and extraction***
119 Filters were treated with an RNA preserve solution and stored in a -80°C freezer.
120 The RNA preserve is a custom made solution of 20 mM EDTA, 0.3 M sodium citrate,
121 and 4.3 M ammonium $SO_4^{2-}$ (pH 5.2). The solution was autoclaved prior to sample
122 application. Total protein, together with total DNA and RNA, was extracted using 2X
123 CTAB lysis buffer and phenol/chloroform (pH=6.5-6.9), and re-suspended in 1 TE-buffer
124 (Tris-EDTA, pH = 8) and stored in 1.5-mL Eppendorf tubes at −20°C. Extraction of
125 biomolecules is further described elsewhere (Lau *et al.* 2014, 2016).
126 ***Amplicon Sequencing and Annotation***
127 The V6 region of archaeal 16S rDNA molecules from the 2011 and 2012 time
128 points was amplified using 958F (AATTGGANTCAACGCCGG) and 1048R
129 (CGRCRGCCATGYACCWC) primers. The V4-V5 region of archaeal 16S rDNA
130 molecules from all time points was amplified using the 517F
131 (GCCTAAAGCATCCGTAGC; GCCTAAARCGTYCGTAGC;
132 GTCTAAAGGGTCYGTAGC; GCTTAAAGNGTYCGTAGC;
133 GTCTAAARCGYYCGTAGC) and 958R (CCGGCGTTGANTCCAATT) primers. For
134 both amplicon datasets, forward primers included 5-nt multiplexing barcodes and a
135 reverse 6-nt index. Triplicate PCR amplifications were performed in 33-µL reaction
136 volumes with an amplification cocktail containing 10.0 U Platinum Taq Hi-Fidelity
137 Polymerase (Invitrogen, Carlsbad, CA), 1X Hi-Fidelity buffer, 200 µM dNTP PurePeak
138 DNA polymerase mix (ThermoFisher), 2 mM $MgSO_4$ and 0.3 µM of each primer. We
139 added approximately 10-25 ng template DNA to each PCR and ran a control without
140 template DNA for each primer pair. Amplification conditions were: initial 94°C, 3

141 minute denaturation step; 25 cycles of 94°C for 30 s, 60°C for 45 s, and 72°C for 60 s;
142 and a final 2 minute extension at 72°C. The triplicate PCR reactions were pooled after
143 amplification and purified using Qiagen MinElute plates followed by clean up, PicoGreen
144 quantitation and Sage PippinPrep size selection. 101-nt paired-end sequencing was
145 performed on an Illumina HiSeq 1000 at the Marine Biological Laboratory (Woods Hole,
146 MA USA). Only reads that were identical in the overlapping regions of the forward and
147 reverse reads were included for annotation. In the case of V6 data, this filter necessitates
148 an exact match across both the forward and reverse read. Sequences that met the given
149 quality criteria were annotated using GAST (Huse *et al.* 2008) and a GAST-formatted
150 reference set.

151 ***Mapping of Metatranscriptomic Data to V6 Amplicons***

152 Quality filtered RNA reads were mapped to the GAST-annotated V6 amplicons of
153 Be326 Bh2 (Magnabosco *et al.* 2014; Young *et al.* 2017) using BLASTn (percent identity
154 >97%; alignment length > 55 nucleotides (nt)). Reads that mapped positively to V6
155 sequences were assigned a consensus taxonomy based on the top three BLASTn hits.

156 ***Generation of Metagenomic and Metatranscriptomic Datasets***

157 DNA samples from 2011 and 2012 were sequenced at the National Center for
158 Genome Resources (Santa Fe, NM). The 2011 and 2012 metagenomic libraries were
159 prepared from 500 ng of DNA using the KAPA High Throughput Library Preparation Kit
160 (KAPA Biosystems), an insert size of approximately 280 bp, and followed by 8 PCR
161 cycles. Paired-end sequencing (2 × 100 nt) was performed on an Illumina HiSeq 2000.
162 DNA from 2013 was sequenced at Lewis Sigler Institute for Integrative Genomics
163 (Princeton, NJ USA) using an Illumina HiSeq 2500. The metagenomic library was
164 prepared using the TruSeq Rapid SBS Kit, size selected for 380-400 nt, and sequenced
165 using paired-end sequencing (2 × 215 nt).

166 RNA samples from 2011, 2012, 2013, $T_0$, $T_1$, and $T_2$ were sequenced at Lewis
167 Sigler Institute for Integrative Genomics (Princeton, NJ USA) on an Illumina HiSeq 2500
168 platform. Here, metatranscriptomic libraries were prepared using the Ovation RNA-Seq
169 v2 System (NuGEN; San Carlos, CA USA), which involved 15-18 cycles of PCR. The
170 2011 and 2012 RNA samples were sequenced using 141-nt single-end sequencing while
171 the 2013, $T_0$, $T_1$, and $T_2$ RNA samples were sequenced using 200-nt single-end reads.

172 ***Targeted Assembly and Tree Building***

173 Reads were quality filtered and assembled using a targeted assembly pipeline
174 (https://github.com/cmagnabosco/OmicPipelines). In summary, this pipeline involved
175 quality filtering reads using default settings on the fastx toolkit
176 (http://hannonlab.cshl.edu/fastx_toolkit/), targeted assembly of *mcrA* GENEs, protein
177 prediction, alignment of reads to a set of well curated McrA peptides, and the
178 construction of a phylogenic tree from the predicted proteins (PhyML (Guindon *et al.*
179 2010), Best of nearest-neighbor-interchange and subtree-pruning-regrafting, 8 rate
180 categories, -b 100). This procedure was also repeated for the assembly of *mmo* genes
181 using a MMO peptide database.

182 Assembled genes of 200 nt or longer were trimmed to include only the coding
183 region of verified *mcrA* and *mmo* genes. This dataset was used as the reference database
184 (Supplementary Data 2) to map quality-filtered DNA and RNA reads using Bowtie2 (--
185 very-sensitive-local). The coverage was calculated as: (number of reads mapped ×
186 average read length)/length of the reference sequence. For correlation analyses, coverage

187 was normalized by dividing by the total number of reads in the dataset. Pearson
188 correlation coefficients (*r*) were computed in Excel using the CORREL function.
189 ***Protein Identification from UPLC-MS/MS Data***
190 Ultra performance liquid chromatography-tandem mass spectrometer (UPLC-
191 MS/MS) data were analyzed in aggregate using the SEQUEST HT search engine in
192 ProteomeDiscoverer v1.4 (ThermoFisher Scientific) using a custom database containing
193 the translated genes from the targeted assembly and published McrA, pMoA, MmoX and
194 AmoA (Supplementary Data 4). Search parameters included trypsin digestion with up to
195 one missed cleavage, methionine oxidation and cysteine carbamidomethylation. A
196 peptide-level false discovery rate (FDR) of 5% was achieved by using the Percolator
197 node in ProteomeDiscoverer, which utilizes the frequency of matching against a reversed
198 database as a rigorous model of the probability of error in the forward matches at given
199 score thresholds. Proteins identified by matches to one unique peptide per run were
200 tallied.
201 ***Activity assays***
202 During the 2012 and 2013 sampling points, water samples were collected into
203 150-mL serum vials ("biovials") and stored at 4°C. Two days prior to sampling, 100 µL
204 of MilliQ water was added to a 150-mL serum vial that had undergone combustion in an
205 oven at 450°C overnight to deactivate spores. The serum vial was then sealed with a
206 butyl rubber stopper that was cleaned by boiling in 0.1 M NaOH solution for 1 hour,
207 rinsed and left to soak in MilliQ water until use. The serum vials were then crimped and
208 left overnight. The next day, the serum vials were purged and pressurized with filtered
209 $N_2$. The vials were then autoclaved and bubble-wrapped for transport underground. A
210 needle was attached to the end of sterile teflon tubing that was attached to the manifold.
211 Water was allowed to flow to rinse the attachment and needle. After 2 minutes of rinsing,
212 the needle was inserted into the biovial and a second needle was added for pressure relief.
213 Water was allowed to flow into the biovial until the relief needle overflowed. Extensive
214 care was taken to ensure that no visible gas bubble remained in the biovial post-sampling.
215 Two sets of enrichment experiments were performed to monitor the response of
216 the biovial communities to methane and a variety of electron acceptors. Experiment 1
217 contained samples from 2012 and 2013. Samples were incubated in triplicate with $^{13}C$-
218 $CH_4$ and $SO_4^{2-}$ (20 mM) or $^{13}C$-$CH_4$ and $NO_3^-$ (20 mM) for 207 and 185 days,
219 respectively. A control incubation with $^{13}C$-$CH_4$ and no electron acceptors was monitored
220 for 207 days to measure endogenous $^{13}CO_2$ production (Control A). Experiment 2
221 included samples from 2012 and 2013 that were incubated in triplicate with $^{13}C$-$CH_4$ and
222 $SO_4^{2-}$ (20 mM), $NO_3^-$ (20 mM) or $O_2$ (5% v/v). A killed (paraformaldehyde, 4% v/v)
223 control without electron acceptors (Control 1) and a live control without electron acceptor
224 or donor were included (Control 2). All samples of Experiment 2 were incubated and
225 monitored over a 43-day period.
226 The samples for all experiments were prepared in 14-mL serum vials sealed with
227 butyl rubber stoppers and aluminum caps. Prior to sample addition, vials were made
228 anoxic by exchanging headspace gas with $N_2$ for 10 cycles and left pressurized (0.5 bar
229 overpressure). 10 mL aliquots of fracture fluid were then added to the vials in an anoxic
230 chamber and amended with the treatments described above. When $^{13}C$-$CH_4$ was added,
231 $N_2$ was added to a pressure of 130 kPa and 99.99% $^{13}C$-$CH_4$ gas (Campro Scientific,
232 Veenendaal, The Netherlands) was added to a final pressure of 180 kPa. Oxygen was

added afterwards, when applicable. All electron acceptor solutions were sterile and anoxic. The serum bottles were statically incubated at 37°C in the dark.

$NO_3^-$ and $SO_4^{2-}$ were analysed using an ion chromatography system equipped with an Ionpac AS9-SC column and an ED 40 electrochemical detector (Dionex, Sunnyvale, CA). The system was operated at a column temperature of 35°C, and a flow rate of 1.2 ml $min^{-1}$. Eluent consisted of a carbonate/bicarbonate solution (1.8 and 1.7 mM respectively) in deionized water. Headspace gas composition was measured on a gas chromatograph-mass spectrometer (GC-MS) composed of a Trace GC Ultra (Thermo Fisher Scientific, Waltham, MA) equipped with a Rt-QPLOT column (Restek, Bellefonte, PA), and a DSQ MS (Thermo Fisher Scientific). Helium was used as a carrier gas with a flow rate of 120 ml $min^{-1}$ and a split ratio of 60. The inlet temperature was 80°C; the column temperature was set at 40°C and the ion source temperature was 200°C. $CH_4$ and $CO_2$ in the headspace were quantified from the peak areas in the gas chromatographs. The fractions of $^{13}CO_2$, $^{13}CH_4$ and $^{12}CH_4$ were derived from the mass spectrum (Shigematsu *et al.* 2004). Validation of the method was done using standards with known mixture of $^{13}CO_2$ and $^{12}CO_2$. The concentrations of total $CO_2$, total $CH_4$, and $^{13}CO_2$ were calculated following the method of Timmers *et al.* (2015). The pressure of the serum vials was determined using a portable membrane pressure unit (GMH 3150, Greisinger electronic GmbH, Regenstauf, Germany). The pH was checked by a standard pH electrode (QiS, Oosterhout, The Netherlands).

**Results and Discussion:**

***A changing fluid chemistry over time***

Over a period of 2.5 years, water isotope analysis revealed large changes in the fracture fluid's $\delta^2H$ and $\delta^{18}O$ isotopic signatures (Fig. 1; purple squares). These changes are inconsistent with contamination with service water in the mine and, instead, indicate mixing of different fracture waters within the system. In 2011, the $\delta^{18}O$ and $\delta^2H$ values were on the global meteoric water line (GMWL) and are indicative of paleometeoric water. This isotopic signature is consistent with other fluids located approximately 1,000 to 1,500 mbls in the Witwatersrand Formation (South Africa) (Fig. 1; green triangles) (Onstott *et al.* 2006; Sherwood Lollar *et al.* 2007). In 2012 and 2013, the $\delta^{18}O$ and $\delta^2H$ signatures of the fluids moved away from the GMWL, indicating mixing with more ancient fluids (Frape *et al.* 1984). A few meters away, Be326 Bh1 (a borehole located in the same mine and depth as the Be326 borehole of this study) exhibited a similar trend in $\delta^{18}O$ and $\delta^2H$ signatures over time—shifting away from the GMWL in 2012 and 2013 (Fig. 1; red diamonds). The displacements between the 2011/2012 and 2012/2013 $\delta^{18}O$ and $\delta^2H$ signatures of the two boreholes are in opposite directions—a pattern that would not be expected if the native fracture fluids were mixing with the mine's service water during this period. Measurements of the fracture fluid's $\delta^2H$ and $\delta^{18}O$ isotopic signatures over the 2-week study were not obtained.

Geophysico-chemical measurements were made for both the 2.5-year and 2-week time series (Table 1). Temperature, pH, and $CH_4$ concentrations were relatively unchanged in both of the time series but the degree to which $E_h$, $SO_4^{2-}$, $NO_3^-$, and $H_2$ concentrations changed was much greater over the 2.5 years (Table 1a). Within the 2.5-year time series, the fracture fluids shifted from a more reduced state ($2011_{Eh}$ = -98 mV, $2011_{[H2]}$ = 130 nM) with limited electron acceptor availability ($2011_{[Sulph.]}$ = 137μM,

279 $2011_{[Nitr.]}$ = 0.4 μM) to a more oxidized state ($2013_{Eh}$ = 21±28 mV, $2013_{[H2]}$ = 25 nM)
280 with much greater electron acceptor availability ($2013_{[Sulph.]}$ = 479 μM, $2013_{[Nitr.]}$ = 4.5
281 μM). The 2-week time series did not exhibit as large of a shift in electron acceptor
282 availability as the 2.5-year time series and maintained a positive $E_h$ throughout (Table
283 1b).
284 ***Microbial community of Be326***
285 The microbial communities of the 2011 and 2012 time points have been reported
286 to be dominated by bacteria (98.5%) (Simkus *et al.* 2015) with the majority being related
287 to Proteobacteria (Magnabosco *et al.* 2014). In order to investigate the community
288 composition of the less numerous archaea, 16S rDNA amplicon sequencing of the
289 archaeal V4-V5 hypervariable region was performed across all time points (Fig. 2a). For
290 the long-term study (2011, 2012, 2013), the archaeal community shifted from an ANME-
291 1- and Methanomicrobia-dominated community in 2011 to a Miscellaneous
292 Crenarchaeotic Group-dominated community in 2012 and a Halobacteria-dominated
293 community in 2013. For the short-term study ($T_0$, $T_1$, $T_2$), there were no noticeable
294 changes between $T_1$ and $T_2$. A slight increase in Halobacteria and a decrease in ANME-1
295 with respect to $T_1$ and $T_2$ were observed in the $T_0$ time point. There is a noticeable
296 difference between the $T_0$, $T_1$, $T_2$ samples community profiles and the 2013 community
297 profile, despite being collected over the same two-week period. However, the filters used
298 in the $T_x$ and 2013 filtrations have varied pore sizes, geometries, and casings and should
299 not be directly compared.
300 Around 1% of V4-V5 amplicons were related to "*Ca.* M. nitroreducens" in all
301 time points except for the 2011 dataset that contained only 2 archaeal amplicons relating
302 to "*Ca.* M. nitroreducens" (Supplementary Data 1). These relative abundances of "*Ca.* M.
303 nitroreducens" are lower than what was reported using archaeal V6 primers on 2011 and
304 2012 samples. With archaeal V6 primers, "*Ca.* M. nitroreducens" accounts for 1.5% of
305 the archaeal community in 2011 and 10.6% of the archaeal community in 2012, while
306 ANME-1 accounts for ~10% of the archaeal community at each time point (Young *et al.*,
307 2017; Supplementary Fig. S1). Despite differences in the relative abundances of taxa
308 based on the primers used, community membership does not appear to be significantly
309 different between the 2 primer sets.
310 In order to estimate the relative activity of each taxonomic group,
311 metatranscriptomic data from each sample were mapped to a database of Be326 Bh2 16S
312 rDNA V6 bacterial (Magnabosco *et al.* 2014) and archaeal (Young *et al.* 2017)
313 sequences. The V6 sequences were selected over the V4-V5 sequences due to their
314 shorter length and stringent quality filtering procedure (see Materials & Methods).
315 Proteobacteria within the family Rhodocyclaceae dominated all of the RNA datasets
316 except for the 2011 dataset that was dominated by Hydrogenophilaceae. The number of
317 bacterial and archaeal species (unique hits within the 16S rDNA V6 database) observed
318 in the metatransciptomic data ranged from 204 in 2013's $T_0$ time point to 414 in the 2012
319 sample (Table 2). MO archaea and bacteria account for only a small percentage of the V6
320 rRNA sequences identified in the metatranscriptomic data (0.3-3%). Notably, the number
321 of species observed in each metatranscriptome's V6 rRNA pool was not correlated to the
322 number of reads generated for each metatranscriptome ($R^2 < 0.01$); however, the number
323 of species observed in each metatranscriptome is almost 10 times less than the number of

324 $OTU_{0.97}$ obtained from the bacterial 16S rDNA V6 dataset (2,478 in 2011 and 3,987 in
325 2012) (Magnabosco *et al.* 2014).
326 ***A detectable shift in the MO community over time***
327 As the organisms responsible for $CH_4$ oxidation in Be326 were present at
328 relatively low abundances, a targeted assembly pipeline
329 (https://github.com/cmagnabosco/OmicPipelines) that employs the PRICE assembler
330 (Ruby, Bellare and DeRisi 2013) was implemented to assemble methyl-coenzyme M
331 reductase (*mcrA*)—the gene for the first step in the anaerobic oxidation of methane
332 (AOM) (Thauer 2011) or the last step in methanogenesis—and a suite of $CH_4$
333 monooxygenases (*mmo*) that are known to play a role in aerobic oxidation of methane
334 (McDonald *et al.* 2008) from the metagenomic and metratranscriptomic datasets.
335 Notably, *mcrA* was selected as an indicator for ANME presence because its phylogeny is
336 congruent with MO phylogeny.
337 Following targeted assembly and annotation, two complete *mcrA* genes related to
338 ANME-1 and "*Ca.* M. nitroreducens", an ANME-2d, were assembled. Only one
339 complete *mmo* gene closely related to *Methylococcus capsulatus* was recovered from the
340 metagenomic and metatranscriptomic data (Fig. 2b, Supplementary Data 2). Partial *mcrA*
341 related to Methanomicrobia and Methanobacteria were also identified in the high-
342 throughput data (Fig. 2b, Supplementary Data 2), but partially assembled *mmo*-related
343 genes were omitted in downstream analyses due to the difficulty in distinguishing *mmo*
344 from homologous ammonia monooxygenases genes (Holmes *et al.* 1995).
345 Assembled *mcrA* and *mmo* were translated into peptide sequences
346 (Supplementary Data 3). Notably, the Be326 "*Ca.* M. nitroreducens"-type McrA was
347 99% identical to the McrA of the reference "*Ca.* M. nitroreducens" genome
348 (Supplementary Data 3, 4). Metaproteomic data were searched against the collection of
349 assembled McrA and MMO and a database of known McrA and MMO peptide sequences
350 (Supplementary Data 4) to confirm that the transcribed genes were translated into
351 proteins. The predicted amino acid sequences (Supplementary Data 3) from the
352 assembled ANME-1, "*Ca.* M. nitroreducens", and *Methylococcus* genes were all
353 identified within the metaproteomic data (Fig. 3, Supplementary Data 5) which further
354 confirmed the presence and activity of these groups of organisms.
355 The abundances (based on coverage) of each MO gene (*mcr,A mmo*) and MO 16S
356 SSU rRNA gene were calculated using Bowtie2 (Langmead and Salzberg 2012) (-very-
357 sensitive-local) and BLASTn, respectively. These analyses provided evidence that the
358 dominant members of the MO community in the metagenomes and metatranscriptomes
359 shifted from ANME-1 to "*Ca.* M. nitroreducens" during the 2.5-year sampling period
360 (Fig. 2) but remained constant during the 2-week sampling period (Supplementary Table
361 1). These observations were consistent with the relative changes in geochemistry over
362 both time scales (Table 1). Notably, "*Ca.* M. nitroreducens" accounted for ≤1% of the
363 archaeal community, as revealed using archaeal V4-V5 16S rDNA primers (Fig. 1),
364 which is in contrast to the higher estimates of "*Ca.* M. nitroreducens" found when using
365 archaeal V6 16S rDNA (Young *et al.*, 2017; Supplementary Fig. S1), metagenomic and
366 metatranscriptomic data. This discrepancy suggests that "*Ca.* M. nitroreducens"
367 sequences are recovered at a lower efficiency in archaeal V4-V5 16S SSU rRNA gene
368 surveys relative to archaeal V6 16S SSU rRNA gene surveys, metagenomic and
369 metatranscriptomic studies.

370 When metagenomic MO *mcrA* and *mmo* abundances of the long-term study
371 (Supplementary Table 2) were correlated to geophysico-chemical measurements, "*Ca.* M.
372 nitroreducens" was positively correlated to $NO_3^-$ ($R^2$=0.99) and $SO_4^{2-}$ ($R^2$=0.98)
373 concentrations but negatively correlated to $CH_4$ ($R^2$=0.99) and $H_2$ ($R^2$=0.99)
374 concentrations. ANME-1 *mcrA* abundances showed an opposite trend and were positively
375 correlated to $CH_4$ ($R^2$=0.96) and $H_2$ ($R^2$=0.97) concentrations but negatively correlated
376 $NO_3^-$ ($R^2$=0.88) and $SO_4^{2-}$ ($R^2$=0.85) concentrations (Table 3). Correlation of
377 metatranscriptomic 16S rRNA and *mcrA* and *mmo* abundances to geophysico-chemical
378 measurements exhibited similar trends (Supplementary Table 3) and are consistent with a
379 transition from an ANME-1-dominated MO community to a "*Ca.* M. nitroreducens"-
380 dominated community. As $NO_3^-$-coupled $CH_4$ oxidation is more energetic than $SO_4^{2-}$-
381 coupled $CH_4$ oxidation (Caldwell *et al.* 2008), an energetic advantage, presumably,
382 provides "*Ca.* M. nitroreducens" a competitive advantage against ANME-1 when $NO_3^-$
383 concentrations are sufficient.
384 $O_2$ concentrations in 2011 and 2013 were below detection limit (Table 1) but were
385 detectable in 2012 (0.47 μM). Likely related to the increased availability of $O_2$, aerobic
386 *Methylococcus*-related *mmo* genes exhibited their highest relative abundances within
387 metagenomic and metatranscriptomic MO gene profiles during 2012 and a minimal
388 presence throughout the remainder of the time points (Fig. 2, Supplementary Table 1).
389 "*Ca.* M. nitroreducens" was the dominant member (73.2±2.8%) of the MOs community
390 during the 2-week time series (Supplementary Table 1) when fracture fluids contained
391 high concentrations of $SO_4^{2-}$ (496±36 μM) and $NO_3^-$ (4.8±0.9 μM) along with a positive
392 $E_h$ (21±28 mV).
393 The correlations between MO abundances and fluid chemistry suggest that a
394 relationship between electron acceptor availability and populations of MOs exists. We
395 therefore wanted to experimentally validate the response of the MOs to changes in
396 electron acceptor availability. As ANME-1, "*Ca.* M. nitroreducens", and *Methylococcus*
397 are best described as a $SO_4^{2-}$-dependent ANME (Wegener *et al.* 2015), $NO_3^-$-dependent
398 ANME (Haroon *et al.* 2013), and aerobic methanotrophs (Kleiveland *et al.* 2012),
399 respectively, we designed experiments to test whether or not each MO lifestyle would
400 respond to an increase in the aforementioned electron acceptor.
401 ***Validation of the MO community through $^{13}CH_4$ enrichments***
402 To better understand the response of the MO community to changes in electron
403 donor/acceptor balance, two sets of $^{13}C$-$CH_4$ laboratory enrichment experiments were
404 performed on fracture water collected in 2012 and 2013. The first experiment
405 (Experiment 1) was a long-term experiment analyzed over 207* days and contained
406 fracture fluid samples from 2012 and 2013 enriched with either $^{13}C$-$CH_4$ and no
407 additional electron acceptor (endogenous activity control), $^{13}C$-$CH_4$+$SO_4^{2-}$ (to stimulate
408 $SO_4^{2-}$-dependent AOM), or $^{13}C$-$CH_4$+$NO_3^-$ (to stimulate $NO_3^-$-dependent AOM). A
409 second set of 2012 and 2013 fracture fluid enrichments (Experiment 2) was analyzed for
410 43 days. Experiment 2 contained $^{13}C$-$CH_4$ treatments of $^{13}C$-$CH_4$+formaldehyde (4%,
411 v/v) (killed control) to rule out non-biological sources of $^{13}C$-$CH_4$ production, $^{13}C$-
412 $CH_4$+$SO_4^{2-}$, $^{13}C$-$CH_4$+$O_2$ (to simulate aerobic methane oxidation), and $^{13}C$-$CH_4$+$NO_3^-$ as
413 well as an electron acceptor- and donor-free control (methanogenesis control). The

* The long term $^{13}C$-$CH_4$+$NO_3^-$ enrichments were run for 183 days.

414 methanogenesis control was intended to detect whether or not methanogenesis, and
415 therefore also trace $CH_4$ oxidation (TMO),was occurring within the samples (Zehnder
416 and Brock 1979). Due to the limited amount of sample, we were unable to test the
417 potential occurrence of $Mn^{4+}$-or $Fe^{3+}$-driven methane oxidation.
418 Unlike the correlations observed between expression data and geochemical
419 parameters, an increase in the proportion of $^{13}C$-$CO_2$ relative to total $CO_2$ (%$^{13}C$-$CO_2$) in
420 the $^{13}CH_4$ enrichments over time provides definitive evidence of $^{13}CH_4$ oxidation under
421 different conditions. Notably, we chose to express our results as %$^{13}C$-$CO_2$ rather than
422 the absolute concentration (molar) of $^{13}C$-$CO_2$ to account for $CO_2$ production from other
423 substrates. In Experiment 1, the $^{13}C$-$CH_4$+$NO_3^-$ enrichments exhibited the greatest rate of
424 %$^{13}C$-$CO_2$ production and, in 2012, the rate of %$^{13}C$-$CO_2$ production (0.017±0.005 %$^{13}C$-
425 $CO_2$ day$^{-1}$) was found to be significantly greater (paired one-tailed Student t-test; $p$=0.02)
426 than in Control A (0.004±0.001 %$^{13}C$-$CO_2$ day$^{-1}$) (Fig. 4). No samples from Experiment
427 2 exhibited an increase in %$^{13}C$-$CO_2$ production (Supplementary Data 5).
428 Although ANME-1 were present in the metatranscriptomic and metaproteomic
429 data during the 2012 and 2013 sampling points, there was not a significant difference in
430 %$^{13}C$-$CO_2$ production between Experiment 1's $^{13}C$-$CH_4$+$SO_4^{2-}$ incubations and the
431 endogenous activity controls (Fig. 4). TMO was probably not responsible for the $^{13}C$-$CO_2$
432 production in the endogenous activity controls of Experiment 1; only the methanogenesis
433 control of the 2013 sample showed minor methanogenesis (and thus TMO) activity
434 (Supplementary Data 5). It is conceivable, however, that $SO_4^{2-}$-dependent AOM occurred
435 in both the endogenous controls and $^{13}C$-$CH_4$+$SO_4^{2-}$ incubations, as the concentrations of
436 $SO_4^{2-}$ in the controls ([$SO_4^{2-}{}_{2012}$] = 623 μM; [$SO_4^{2-}{}_{2013}$] = 479 μM) are well within the
437 lower range of $SO_4^{2-}$ concentrations (100-1200 μM) that have been reported for $SO_4^{2-}$-
438 coupled AOM (Beal, Claire and House 2011; Segarra *et al.* 2015). Combined, these
439 findings suggest that $SO_4^{2-}$-coupled AOM likely occurred in the controls of Experiment 1
440 and 2.
441
442 **Conclusions:**
443 Metagenomic, metatranscriptomic, and metaproteomic data suggest that
444 community composition, activity, and function are changing in response to natural
445 fluctuations in fluid chemistry. The observed $CH_4$ oxidation in the controls and
446 dominance of ANME-1 in the 2011 samples (when $SO_4^{2-}$ concentrations were lowest)
447 indicate that the *in situ* fluids contain enough $SO_4^{2-}$ to power $SO_4^{2-}$-coupled MO. The
448 increase in %$^{13}C$-$CO_2$ production in the $^{13}C$-$CH_4$+$NO_3^-$ enrichments and correlation of
449 "*Ca.* Methanoperedens" abundances to electron acceptor concentrations *in situ* suggest
450 that electron acceptor availability plays an important role in MO population dynamics.
451 Together, these results provide the most conclusive biological evidence to date that $CH_4$
452 oxidation occurs and is an integral component of the deep terrestrial subsurface carbon
453 cycle.
454
455 **Data Availability:**
456 Metagenomic and metatranscriptomic data are available at NCBI BioProject
457 PRJNA308990. 16S amplicon data are available under NCBI BioProject PRJNA263371.
458
459

**Tables and Figures:**

**TABLE 1a. Geophysico-chemical measurements for the long-term study**

| | **2011** | **2012** | **2013** |
|---|---|---|---|
| **Dates Sampled** | Jan 21-27, 2011 | July 12-27, 2012 | Aug 1-15, 2013 |
| **Temperature (°C)** | 36.9 | 37.3±1.2 | 35.1±0.8 |
| **pH** | 8.83 | 8.55 | 8.17±0.7 |
| **$E_h$ (mV)** | -98 | -27.5±6.4 | 21±28 |
| **$SO_4^{2-}$ (µM)** | 137 | 623 | 479 |
| **$NO_3^-$ (µM)** | 0.4 | 6.0 | 4.5 |
| **$O_2$ (Chemet) (µM)** | b.d. | 0.47 | b.d.* |
| **$H_2$ (nM)** | 130 | 9 | 25 |
| **$CH_4$ (mM)** | 2.0 | 0.9 | 1.1 |

b.d. = below detection (<0.31 µM)
b.d.* = below detection (<1.6 µM)

**Table 1b. Geophysico-chemical measurements for the short-term study**

| | **$T_0$** | **$T_1$** | **$T_2$** |
|---|---|---|---|
| **Dates Sampled** | Aug 1, 2013 | Aug 8, 2013 | Aug 15, 2013 |
| **Temperature (°C)** | 35.8 | 35.3 | 28.6 |
| **pH** | 8.2 | 8.1 | 7.9 |
| **$E_h$ (mV)** | 9 | 53 | 1 |
| **$SO_4^{2-}$ (µM)** | 531 | 499 | 459 |
| **$NO_3^-$ (µM)** | 5.3 | 5.3 | 3.7 |
| **$O_2$ (Chemet) (µM)** | b.d.* | b.d.* | b.d.* |
| **$H_2$ (nM)** | $5.8\times10^{-5}$ | 10.4 | 39.8 |
| **$CH_4$ (mM)** | 0.8 | 1.2 | 1.0 |

b.d.* = below detection (<1.6 µM)

485 **Table 2: Metatranscriptomic species richness observed and estimated by Chao 1**
486 **and ACE metrics and cell concentrations measured in the field.**

| | **2011** | **2012** | **2013** | **$T_0$** | **$T_1$** | **$T_2$** |
|---|---|---|---|---|---|---|
| **Species (S) Observed** | 302 | 414 | 247 | 222 | 204 | 248 |
| **S.Chao1** | 344±22 | 440±10 | 256±7 | 233±9 | 216±8 | 276±16 |
| **S.ACE** | 317±8 | 450±10 | 253±6 | 233±5 | 212±7 | 260±8 |
| **Cell concentration ($\times 10^3$ cells $mL^{-1}$)** | 1.3^-18.3* | 2.2*-31^ | 3.2^ | 3.2^ | n.m. | n.m. |

487 ^DAPI-derived cell concentration
488 *PLFA-derived cell concentration using a conversion factor of $6\times10^4$ cells/pmol PLFA as
489 previously reported in Simkus et al. (2015)
490 n.m. = not measured
491
492
493
494
495
496
497 **Table 3:** Correlation ($R^2$) between normalized metagenomic *mcrA* or *mmo* PEG coverage
498 and geochemical parameters. Positive correlations are underlined.
499

| | | **$NO_3^-$** | **$SO_4^{2-}$** | **$CH_4$** | ***$E_h$*** | **pH** | **$H_2$** |
|---|---|---|---|---|---|---|---|
| **2.5-Year Time Series** | "*Ca.* Methanoperedens" | 0.99 | 0.98 | 0.99 | 0.70 | 0.52 | 0.99 |
| | ANME-1 | 0.88 | 0.85 | 0.93 | 0.90 | 0.76 | 0.95 |
| | *Methylococcales* | 0.12 | 0.14 | 0.07 | 0.10 | 0.25 | 0.05 |

500
501
502
503
504
505
506

**Figure 1. $\delta^2H_{H2O}$ and $\delta^{18}O_{H2O}$ for Beatrix (Be) Gold Mine fracture fluids.**

This figure plots the $\delta^{18}O$ (x-axis) against the $\delta^2H$ (y-axis) for each of the three time points (purple squares) in the long-term study of Be326 (2011, 2012, 2013). The black diagonal line represents the global meteoric water line (Craig 1961) (GMWL). The 2011 sample sits on the GMWL, consistent with historic Be datapoints (green triangles) and paleometeoric water (Lippmann *et al.* 2003; Ward *et al.* 2004). The 2012 and 2013 time points are displaced away from the GMWL along trends that have been observed to be consistent with mixing with older, more saline fracture fluids (Ward *et al.* 2004; Sherwood Lollar *et al.* 2007). The dotted blue lines indicate possible mixing patterns. Be326_Bh1 (red diamonds) is a borehole located in the same mine and at the same depth as the borehole sampled in this study. EV=Evander Mine; KL=Kloof. Data for EV, KL, and Adams are adapted from Ward *et al.* (2004).

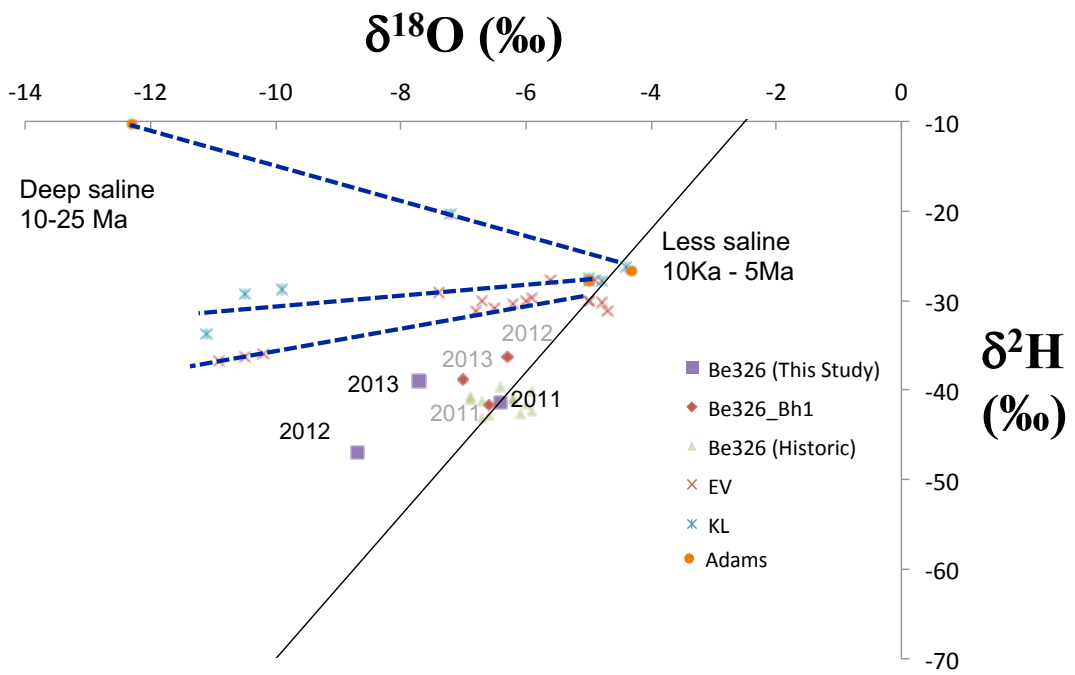

**Figure 2. Change in the $CH_4$ oxidizing community and activity over time.** a) The relative abundance (bar height) of major archaeal groups (colors of bars) identified in the archaeal V4-V5 16S rDNA surveys are shown. b) A phylogenetic tree was constructed using PhyML from a McrA peptide database (Supplementary Data 6) and the predicted proteins from the *mcrA* targeted assembly (designated by a *). The predicted MMO from the targeted assembly is also displayed. The 2×3 blocks represent the relative abundance of each taxon (DNA, left column; RNA, right column) with respect to their $CH_4$-related protein of interest (McrA or MMO) over time (row 1, 2011; row 2, 2012; row 3; 2013). Notably, Methanobacteria-related McrA PEGs were selected as the outgroup in this presentation of the McrA phylogenetic tree due to Methanobacteria's placement in species tree of Euryarchaeota.

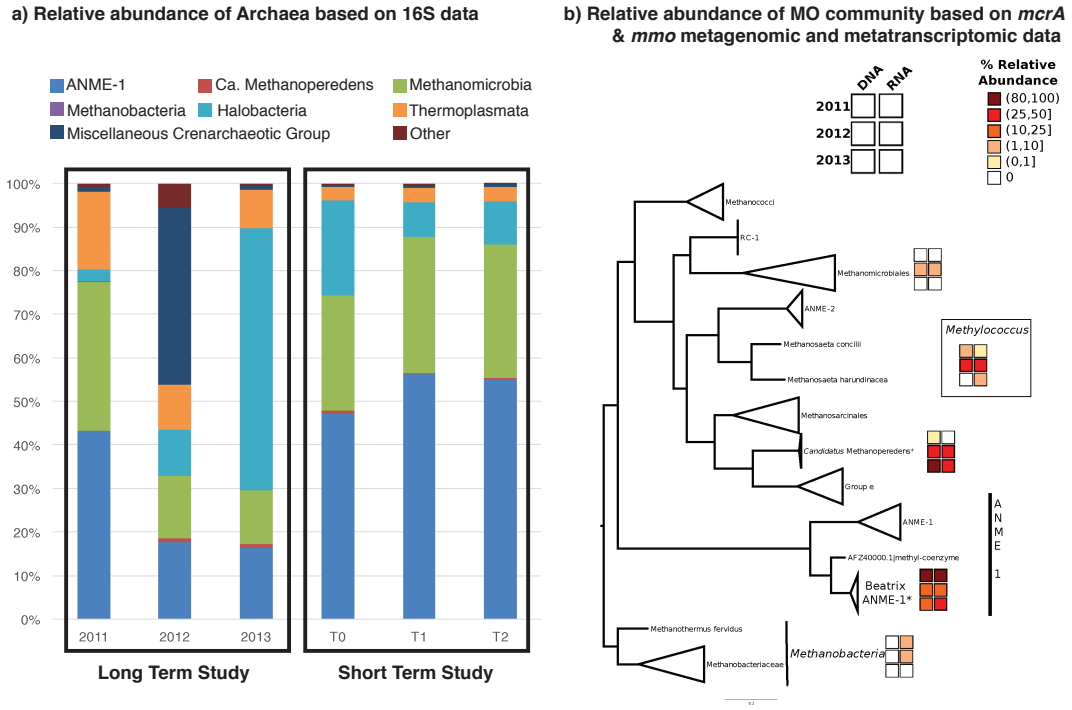

555 **Figure 3: Peptide mapping to identified McrA and MMO proteins**

556

A)

```
      1         10        20        30        40        50
      |         |         |         |         |         |
  1   MPHRDAQHSFLKAMSDKFVEKPESTKTKFYVYGSKDPRYAVGGLAQKGAF
 51   RKREFIDDAAKIVAERVQGTPAYNPDVGMPQGQRFLMPYILNHTDIMCYH
101   DDLHVVNNAAMQQAWDDMRRTIVLGLDDAHGILETRLGKEVTPDTINHYL
151   EVCNHCLPGAALIQEHMVETKPALVADSYVKVFTGDDDLADALDRRMLLD
201   INKEFPAGWEKPGEQADQLKGTIGKKLWQALYMPTIVGRMTDGGTMFRWV
251   GMQVGMTMINAYKVCAGESATGEFAFMAKHASVVMMANYMPVRRARAQNE
301   PGGLPLGICCDCTRSPALFPMDPVRAELEAIAIGALVYDQLWFGIYMSGG
351   VGFTQYASATYTDNILEDFCYKGDEIAIDMFGERGKAEPTMENIEKLTRA
401   GSDYCLTQYEAYPTVAESHFGGSVRAACQSAGAATCVASATADAQAALNS
451   WALAQLLHYASVGRLGFYGYDLQDQCTSSTSFAYRSDEGLPFEMRGVNYP
501   NFAMNVGHQSAYAGLNAGAHLSRKDAWVLSPLIKVAFSDRDLPFDWGYTT
551   REYGRGALREFKPAGERDLIIP
```

T Threonine substituted for Alanine in 4 of the 8 assembled PEGs
Peptides (13) unique to ANME-1 sequences assembled in this study
Peptides (1) shared with an uncultured archaeon GZfos19C7 (AAU82711.1)

B)

```
      1         10        20        30        40        50
      |         |         |         |         |         |
  1   VSQMAEPRFKKAMETKYAKEWGTNKCGSTAKSKITDKKTKYLRLGYTQNP
 51   RKVEMTKCGAAITKKRGLQAYDPKLHLAGIPMGQRQLTPYTISGTDIVCD
101   GDDLHFVNNAAMQQEWDDIRRTCIVGLDLAHETLEKRLGKEVTPETINYY
151   LEVLNHAMPGAAIVQEHMVETHPALVDDCYVKVFTGDETLQDEIDKQFVI
201   NIDNEFPAEQAKQIKAGIGKTSWQAVHIPTIVTRTEDGPGTSRWMAMQVG
251   MTFISAYHMCAGEAAVGELAFTAKHAGLVEMSDMIPARRARGPNEPGGLS
301   FGHMADIVQTSRKTPDDPVNVALQTASAASMLYDQIWLGGYMSGGVGFTM
351   YATPAYTNDILDDYVYWGADYAQKKYGKFGSAKATIETVKDIGTEVTLYG
401   IEAYEKYPTTLEDHFGGSQRATVLAIAAGASTAMATGHSNAGLSAWYLSM
451   YLHKEAWGRLGFYGYDLQDQCGATNVFSLGSDEGAIGEVRGANYPNYAMN
501   VGHQGGYTTVVSAAHAGKKDAFCVNPLVKSCFADDLVNFDFADPRGAFGK
551   AALREWDRCAGERAFVIPAK
```

Q Glutamine substituted for Lysine in 2 of the 6 assembled PEGs
V Valine substituted for Glycine in 2 of the 6 assembled PEGs
A Alanine substituted for Aspartic Acid in 2 of the 6 assembled PEGs
Peptides (8) unique to *Ca.* Methanoperedens nitroreducens (WP_048089615.1)
Peptides (1) shared with *Methanococcoides methylutens* (WP_048204805.1)
Peptides (1) shared with *Methanomethylovorans hollandica* (WP_015325028.1)

C)

```
      1         10        20        30        40        50
      |         |         |         |         |         |
  1   MKTIKDRIAKWSAIGLLSAVAATAFYAPSASAHGEKSQAAFMRMRTIHWY
 51   DLSWSKEKVKINETVEIKGKFHVFEGWPETVDEPDVAFLNVGMPGPVFIR
101   KESYIGGQLVPRSVRLEIGKTYDFRVVLKARRPGDWHVHTMMNVQGGGPI
151   IGPGKWITVEGSMSEFRNPVTTLTGQTVDLENYNEGNTYFWHAFWFAIGV
201   AWIGYWSRRPIFIPRLLMVDAGRADELVSATDRKVAMGFLAATILIVVMA
251   MSSANSKYPITIPLQAGTMRGMKPLELPAPTVSVKVEDATYRVPGRAMRM
301   KLTITNHGNSPIRLGEFYTASVRFLDSDVYKDTTGYPEDLLAEDGLSVSD
351   NSPLAPGETRTVDVTASDAAWEVYRLSDIIYDPDSRFAGLLFFFDATGNR
401   QVVQIDAPLIPSFM
```

Peptides (4) unique to *Methylococcus capsulatus* (WP_010961049.1)
Peptides (1) shared with *Methylocaldum szegediense* (WP_026609852.1)

557

558

559 **Figure 4: $^{13}C$-$CO_2$ production after $^{13}C$-$CH_4$ enrichment.**
560 The rates of $^{13}C$-$CO_2$ production (%$^{13}C$-$CO_2$ day$^{-1}$) from the 2012 (gray) and 2013 (black)
561 fluids of Experiment 1 are displayed. The 2012 samples were run in triplicate and the
562 standard deviations are shown. The star above the 2012 CH4+NO3 bar indicates that the
563 rate of $^{13}C$-$CO_2$ production in the $^{13}C$-CH4+$NO_3^-$ enrichment was significantly greater
564 ($p$=0.02) than the electron acceptor-free control (Control A).
565

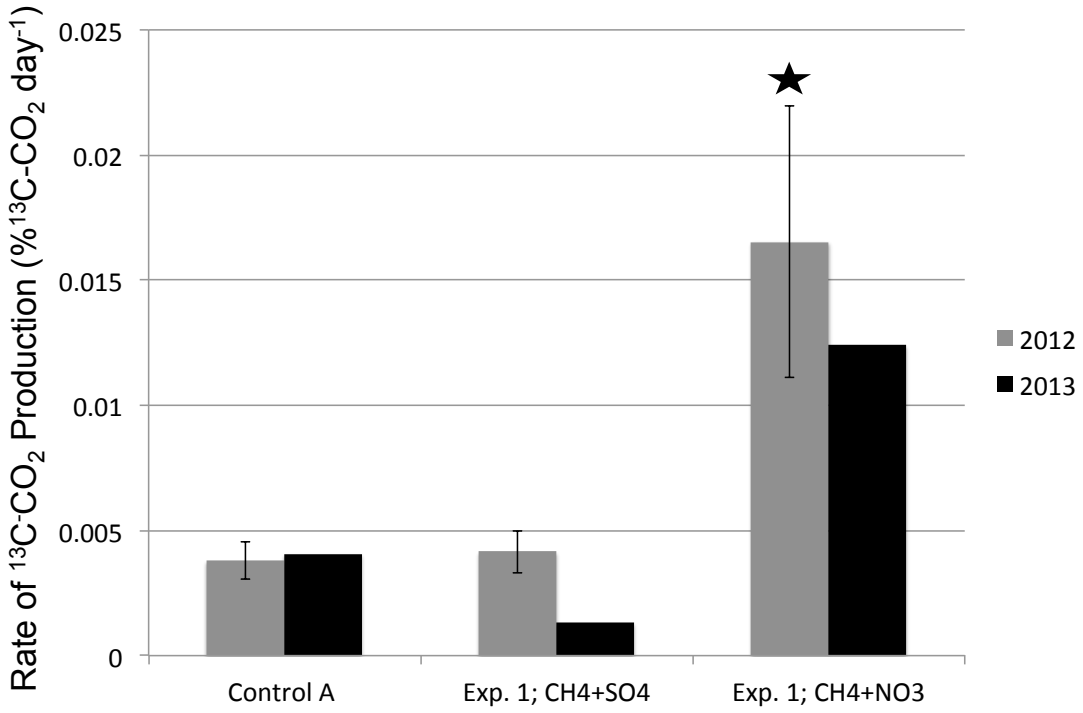


566
567
568
569
570
571
572
573
574
575
576
577
578
579
580
581
582
583
584

585 **Supplement:**
586 Supplementary Figure S1 – Relative abundance of archaeal 16S SSU rRNA gene v6
587 amplicons for the 2011 and 2012 time points
588 Supplementary Table 1 – $CH_4$ oxidizing community with respect to their $CH_4$-related
589 gene
590 Supplementary Table 2 – Normalized coverage $CH_4$-related genes abundances
591 Supplementary Table 3 – Correlation of $CH_4$ oxidizing community activity to fluid
592 chemistry
593 Supplementary Data 1 – Archaeal V4-V5 16S rDNA annotations
594 Supplementary Data 2 – Assembled *mcrA* and *mmo* genes
595 Supplementary Data 3 – Predicted proteins from assembled *mcrA* and *mmo*
596 Supplementary Data 4 – Datasets used for protein mapping
597 Supplementary Data 5 – Protein mapping results
598 Supplementary Data 6 – Enrichment experiment results
599 Supplementary Data 7 – McrA protein library used to generate phylogenetic tree

600 **Acknowledgments**
601 This research was supported by funding from the National Science Foundation to T.C.O.
602 (EAR-0948659) and to TLK (EAR-0948335) and the Deep Carbon Observatory (Alfred
603 P. Sloan Foundation) to M.C.Y.L. (Sloan 2013-10-03, subaward 48045). Research of
604 P.H.A.T. is supported by the Soehngen Institute of Anaerobic Microbiology (SIAM)
605 Gravitation grant (024.002.002) of the Netherlands Ministry of Education, Culture and
606 Science and the Netherlands Organisation for Scientific Research (NWO). Partial support
607 for isotopic analyses was provided by the Natural Sciences and Engineering Research
608 Council of Canada. We are indebted to the logistical support of Sibanye Gold Limited,
609 the management and staff of Beatrix Gold Mine and specifically to S. Maphanga of
610 Beatrix gold mine. We thank Matthew Cahn (Department of Molecular Biology,
611 Princeton University) and the staff of Research Computing (Office of Information
612 Technology, Princeton University), especially Robert Knight, for their technical support
613 with the computational analyses.
614

615 **References**

616 Bagnoud A, Chourey K, Hettich RL *et al*. Reconstructing a hydrogen-driven microbial
617 metabolic network in Opalinus Clay rock. *Nat Commun* 2016;**7**.

618 Beal EJ, Claire MW, House CH. High rates of anaerobic methanotrophy at low sulfate
619 concentrations with implications for past and present methane levels. *Geobiol*
620 2011;**9**:131–9.

621 Caldwell SL, Laidler JR, Brewer EA *et al*. Anaerobic oxidation of methane: mechanisms,
622 bioenergetics, and the ecology of associated microorganisms. *Environ Sci Technol*
623 2008;**42**:6791–9.

624 Daly RA, Borton MA, Wilkins MJ *et al*. Microbial metabolisms in a 2.5-km-deep
625 ecosystem created by hydraulic fracturing in shales. *Nat Microbiol* 2016;**1**:16146.

626 Ettwig KF, Butler MK, Le Paslier D *et al*. Nitrite-driven anaerobic methane oxidation by
627 oxygenic bacteria. *Nature* 2010;**464**:543–8.

628 Ettwig KF, Zhu B, Speth D *et al*. Archaea catalyze iron-dependent anaerobic oxidation of

methane. *Proc Natl Acad Sci* 2016;**113**:12792–6.

Frape SK, Fritz P, McNutt RH t. Water-rock interaction and chemistry of groundwaters from the Canadian Shield. *Geochim Cosmochim Acta* 1984;**48**:1617–27.

Guindon S, Dufayard J-F, Lefort V *et al*. New algorithms and methods to estimate maximum-likelihood phylogenies: assessing the performance of PhyML 3.0. *Syst Biol* 2010;**59**:307–21.

Haroon MF, Hu S, Shi Y *et al*. Anaerobic oxidation of methane coupled to nitrate reduction in a novel archaeal lineage. *Nature* 2013;**500**:567–70.

Holmes AJ, Costello A, Lidstrom ME *et al*. Evidence that participate methane monooxygenase and ammonia monooxygenase may be evolutionarily related. *FEMS Microbiol Lett* 1995;**132**:203–8.

Huse SM, Dethlefsen L, Huber JA *et al*. Exploring microbial diversity and taxonomy using SSU rRNA hypervariable tag sequencing. *PLoS Genet* 2008;**4**, DOI: 10.1371/journal.pgen.1000255.

Kleiveland CR, Hult LTO, Kuczkowska K *et al*. Draft genome sequence of the methane-oxidizing bacterium Methylococcus capsulatus (Texas). *J Bacteriol* 2012;**194**:6626.

Langmead B, Salzberg SL. Fast gapped-read alignment with Bowtie 2. *Nat Methods* 2012;**9**:357–9.

Lau MCY, Cameron C, Magnabosco C *et al*. Phylogeny and phylogeography of functional genes shared among seven terrestrial subsurface metagenomes reveal N-cycling and microbial evolutionary relationships. *Front Microbiol* 2014;**5**.

Lau MCY, Kieft TL, Kuloyo O *et al*. An oligotrophic deep-subsurface community dependent on syntrophy is dominated by sulfur-driven autotrophic denitrifiers. *Proc Natl Acad Sci* 2016:201612244.

Magnabosco C, Tekere M, Lau MCY *et al*. Comparisons of the composition and biogeographic distribution of the bacterial communities occupying South African thermal springs with those inhabiting deep subsurface fracture water. *Front Microbiol* 2014;**5**:679.

McDonald IR, Bodrossy L, Chen Y *et al*. Molecular ecology techniques for the study of aerobic methanotrophs. *Appl Environ Microbiol* 2008;**74**:1305–15.

Morozova D, Wandrey M, Alawi M *et al*. Monitoring of the microbial community composition in saline aquifers during CO 2 storage by fluorescence in situ hybridisation. *Int J Greenh Gas Control* 2010;**4**:981–9.

Morozova D, Zettlitzer M, Let D *et al*. Monitoring of the microbial community composition in deep subsurface saline aquifers during CO 2 storage in Ketzin, Germany. *Energy Procedia* 2011;**4**:4362–70.

Onstott TC, Lin L-H, Davidson M *et al*. The origin and age of biogeochemical trends in deep fracture water of the Witwatersrand Basin, South Africa. *Geomicrobiol J* 2006;**23**:369–414.

Purkamo L, Bomberg M, Nyyssönen M *et al*. Dissecting the deep biosphere: retrieving authentic microbial communities from packer-isolated deep crystalline bedrock

fracture zones. *FEMS Microbiol Ecol* 2013;**85**:324–37.

Rajala P, Bomberg M, Kietäväinen R *et al*. Rapid reactivation of deep subsurface microbes in the presence of C-1 compounds. *Microorganisms* 2015;**3**:17–33.

Ruby JG, Bellare P, DeRisi JL. PRICE: software for the targeted assembly of components of (meta) genomic sequence data. *G3 Genes| Genomes| Genet* 2013;**3**:865–80.

Segarra KEA, Schubotz F, Samarkin V *et al*. High rates of anaerobic methane oxidation in freshwater wetlands reduce potential atmospheric methane emissions. *Nat Commun* 2015;**6**.

Sherwood Lollar B, Voglesonger K, Lin L-H *et al*. Hydrogeologic controls on episodic H2 release from Precambrian fractured rocks-Energy for deep subsurface life on Earth and Mars. *Astrobiology* 2007;**7**:971–86.

Shigematsu T, Tang Y, Kobayashi T *et al*. Effect of dilution rate on metabolic pathway shift between aceticlastic and nonaceticlastic methanogenesis in chemostat cultivation. *Appl Environ Microbiol* 2004;**70**:4048–52.

Simkus DN, Slater GF, Lollar BS *et al*. Variations in microbial carbon sources and cycling in the deep continental subsurface. *Geochim Cosmochim Acta* 2015.

Thauer RK. Anaerobic oxidation of methane with sulfate: on the reversibility of the reactions that are catalyzed by enzymes also involved in methanogenesis from CO 2. *Curr Opin Microbiol* 2011;**14**:292–9.

Timmers PHA, Gieteling J, Widjaja-Greefkes HCA *et al*. Growth of anaerobic methane-oxidizing archaea and sulfate-reducing bacteria in a high-pressure membrane capsule bioreactor. *Appl Environ Microbiol* 2015;**81**:1286–96.

Wegener G, Krukenberg V, Riedel D *et al*. Intercellular wiring enables electron transfer between methanotrophic archaea and bacteria. *Nature* 2015;**526**:587–90.

Young ED, Kohl IE, Lollar BS *et al*. The relative abundances of resolved l2 CH 2 D 2 and 13 CH 3 D and mechanisms controlling isotopic bond ordering in abiotic and biotic methane gases. *Geochim Cosmochim Acta* 2017;**203**:235–64.

Zehnder AJ, Brock TD. Methane formation and methane oxidation by methanogenic bacteria. *J Bacteriol* 1979;**137**:420–32.